Geoderma 424 (2022) 115987

Contents lists available at ScienceDirect

Geoderma

journal homepage: www.elsevier.com/locate/geoderma

Analysis of heat pulse measurements in double-layered soils with the heating probe positioned at the layer interface

Wei Peng [a], Yili Lu [a,*], Tusheng Ren [a], Robert Horton [b]

[a] College of Land Science and Technology, China Agricultural University, Beijing 100193, China
[b] Department of Agronomy, Iowa State University, Ames, IA 50011, United States

ARTICLE INFO

Handling Editor: Morgan Cristine L.S.

Keywords:
Heterogeneity
Double-layered soils
Heat transfer
Layer interface
Model
Heat pulse

ABSTRACT

In the case where a heat-pulse (HP) sensor installed in a layered soil with the heating and sensing probes positioned at different layers, the HP measurement violates the underlying assumption of soil homogeneity for the cylindrical perfect conductors (CPC) theory that is used to interpret the HP data. In this study, laboratory and numerical studies were performed to evaluate the heat transfer patterns and models to analyze HP measurement data when heating probe was positioned at the interface of a double-layered soil with different upper- and lower-layer properties. A parameterized hetero-CPC model was proposed to describe temperature-by-time curves at the sensing probes in the upper and lower soil layers. The hetero-CPC estimates matched well with the simulated values, and its accuracy relied on the thermal property differences between the soil layers. The heat distributions caused by heat pulse inputs in the layered soils showed semi-circular isotherms with different radii centered on the heating source, therefore showing discrepancies in heat fluxes for the upper and lower soil layers. The proposed hetero-CPC model was able to accurately describe the combined effects of finite probe properties and heterogeneous soil thermal property values on the HP data in a double-layered soil system with the heating probe positioned at the layer interface.

1. Introduction

Soil thermal properties are vital for accurate estimation of surface energy balance and for determination of soil heat transfer process that are embedded in large simulation schemes (Peters-Lidard et al., 1998; He et al., 2018; Xie et al., 2019). The heat-pulse (HP) sensor is a promising tool for measuring soil thermal properties both in laboratory and field conditions (Gamage et al., 2019; Liu et al., 2020). Several algorithms, e.g., the instantaneous infinite line source (IILS), the pulse infinite line source (PILS) and the cylindrical perfect conductors (CPC) models (Campbell et al., 1991; Bristow et al., 1994; Knight et al., 2012; Kluitenberg et al., 1993, Kluitenberg et al., 1995, Kluitenberg et al., 2021), have been proposed to analyze the HP measured temperature-by-time curves for estimating soil heat capacity (C) and thermal conductivity (λ). Among them, the CPC model has been reported to give accurate soil thermal property values, especially for large HP sensors (Kamai et al., 2015; Peng et al., 2019, Peng et al., 2021).

The above algorithms have a common assumption that heat transfer occurs in a homogeneous soil surrounding the HP sensor. Under field conditions, heterogeneous soil properties usually exist within the measurement volume of the HP sensor. Thus, it is essential to examine the performance of these algorithms in heterogeneous soil environments. Philip and Kluitenberg (1999) and Kluitenberg and Philip (1999) evaluated the estimation errors of the HP measurement data due to soil heterogeneity across a plane interface. They derived the approximate IILS solutions to estimate soil thermal property values when a HP probe was installed at different locations relative to the plane interface. Others considered probe and soil configurations with a HP sensor installed near plane interfaces, or they extended the Philip and Kluitenberg (1999) solution by including pulsed heating and adiabatic boundary conditions (Zhang et al., 2014; Xiao et al., 2015; Liu et al., 2020; Sang et al., 2020). To date, the effect of finite probe properties has not been considered in HP data analysis associated with heterogeneous soil conditions, which merits further evaluation.

In practical applications, layered soil properties are most likely to appear in a soil profile, such as the existence of a dry soil layer during evaporation or a wetting front during infiltration processes. The uneven distribution of water and soil properties would cause the differences in soil thermal properties in layered soils, therefore affecting the heat transfer process during HP measurements. Kluitenberg and Philip

* Correspondence author.
E-mail address: luyili@cau.edu.cn (Y. Lu).

https://doi.org/10.1016/j.geoderma.2022.115987
Received 4 January 2022; Received in revised form 2 June 2022; Accepted 5 June 2022
Available online 11 June 2022

(1999) analyzed heat flow and temperature isotherm distributions when the HP sensor was separated by an interface between two regions with different C and λ values, but the regions had the same thermal diffusivity (κ) value. They showed that the presence of an interface affected the temperature distribution in a HP measurement. Isotherms that reached the interface were no longer concentric in the soil layer where the heating source was located but became circular arcs centered on the heating source in the other soil layer. There is a need to evaluate the heat flow, isotherm distributions, and HP measured thermal properties when the heating source was positioned at the interface between two regions with different soil thermal property values.

In this study, we studied heat transfer in heterogeneous soils by considering a special case with the heating probe positioned at the layer interface of a double-layered soil. The dynamic temperature field, heat fluxes, as well as the parameterized PILS and CPC theories were evaluated with both laboratory experiments and numerical simulations.

2. Materials and methods

Laboratory repacked soil column experiments and numerical simulations were performed for the double-layered soil conditions (Fig. 1). First, we parameterized the PILS and CPC theories referring to the Philip and Kluitenberg (1999) solution. Second, the HP sensor measured temperature-by-time curves were compared to those simulated by using the COMSOL Multiphysics finite element software to evaluate the accuracy of the simulated results. Third, numerical simulations with hypothetical soils were performed to analyze heat transfer around the HP sensor, and to evaluate the performance of parameterized theories.

2.1. Parameterization of theories for HP measurements in double-layered soils with the heating probe positioned at the layer interface

In Fig. 1, the line $z = 0$ in the (x, z) plane is the plane interface between two soil layers with different thermal properties. The heating probe (H) of a 3-probe HP sensor is positioned at the layer interface. One sensing probe (S1) locates in the upper soil layer, and another sensing probe (S2) locates in the lower soil layer at distances of z_1 and z_2 away from the interface, respectively. For $z > 0$, soil C, κ, and λ are equal to C_+, κ_+, and λ_+, respectively. For $z < 0$, $C = C_-$, $\kappa = \kappa_-$, and $\lambda = \lambda_-$.

Philip and Kluitenberg (1999) presented an approximate solution (hetero-IILS) for the soil layer condition of Fig. 1 to quantify the errors in

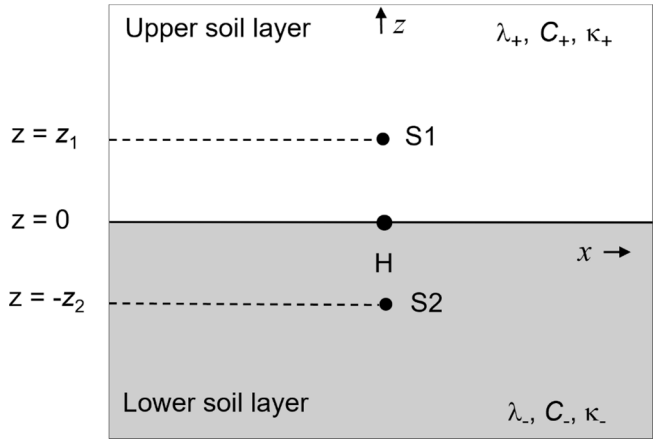

Fig. 1. The heating probe H is positioned at $(x, z) = (0, 0)$ at the interface of a double-layered soil. The upper soil layer has $z > 0$ and soil heat capacity (C), thermal diffusivity (κ), thermal conductivity (λ) equal to C_+, κ_+, λ_+. The lower soil layer has $z < 0$ and $C = C_-$, $\kappa = \kappa_-$, $\lambda = \lambda_-$. The sensing probe S1 is positioned at $(x, z) = (0, z_1)$ above the soil layer interface, and the sensing probe S2 is positioned at $(x, z) = (0, -z_2)$ below the interface. z_1 and z_2 are the distances between the sensing probes and the heating probe, respectively.

HP measurements. The hetero-IILS solution (Eqs. [A1-A2] in the Appendix) was derived from the theory of instantaneous heating, without considering the heat pulse length and the finite probe properties, which might lead to errors in soil thermal property estimates (Bristow et al., 1994; Liu et al., 2013; Knight et al., 2012). In this study, a hetero-PILS solution (Eqs. [A3-A4] in the Appendix) was proposed by substituting the instantaneous heat source in the hetero-IILS solution with a pulsed heat source. Referring to the representation of the hetero-PILS solution, we parameterized the CPC solution as an analogous method, and a hetero-CPC solution (Eqs. [A6-A8] in the Appendix) was proposed for the case of Fig. 1. Details on the hetero-IILS, hetero-PILS and hetero-CPC solutions were provided in the Appendix. The three solutions were used to generate temperature-by-time curves for the measurement scenarios depicted in Fig. 1 with the setting of different thermal property values in the upper and lower soil layers.

2.2. HP measurements on repacked soil columns

Laboratory experiments were performed on repacked soil samples to obtain the measured temperature-by-time curves. The Peng et al. (2019) HP sensor was used in the measurements. The sensor had a probe length of 70 mm and a probe spacing of 10 mm, with dissimilar diameters for the heating (2.38 mm) and sensing (2 mm) probes. This design makes it possible to minimize soil disturbance and probe spacing change during sensor insertion (Peng et al., 2019, Peng et al., 2021). The actual values of probe spacing were estimated by fitting the CPC solution to the temperature-by-time curves obtained in agar-immobilized water (5 g L^{-1}, $C = 4.18$ MJ m^{-3} K^{-1} at 20°C) using the MATLAB software (The Math Works, Inc., Natick, MA) (Peng et al., 2021).

The HP measurements were made on sand (94% sand, 1% silt, 5% clay) and loam (48% sand, 38% silt, 14% clay) soils at a room temperature of 20±1°C. The sand soil was collected from the 0–10 cm layer of a field in Guanting, Beijing City; and the loam soil was collected from the 0–20 cm layer of a field in Jizhou Country, Hebei Province, China. The soils were classified as Entisols soil (USDA Soil Taxonomy). Soil particle-size distributions were measured with the pipette method (Gee and Or, 2002). Soil samples were air dried, passed through a 2-mm sieve, and packed into a cubic (80 × 80 × 80 mm) container with desired θ and ρ_b values. The double-layered soil sample was established by packing the soils with specific θ and ρ_b values in upper and lower soil layers (Fig. 1). The target θ values were 0.05, 0.10, 0.15, and 0.20 m^3 m^{-3} and the ρ_b values were 1.40 and 1.60 Mg m^{-3} for the sand soil, and 1.20 and 1.40 Mg m^{-3} for the loam soil. In total, eight different scenarios were used to create double-layered soil samples for HP measurements (Table 1).

We followed a three-step procedure to prepare the double-layered

Table 1
Eight different scenarios used to represent various thermal property combinations in the double-layered soil columns for COMSOL simulation study. Parameters C_+, κ_+, and λ_+ represent the heat capacity (C), thermal diffusivity (κ), and thermal conductivity (λ) of the upper soil layer, respectively, and C_-, κ_- and λ_- represent the corresponding values of the lower soil layer. Parameter q' indicates the heat input, which was obtained in laboratory heat pulse measurements.

Soil	Scenario	C_+ MJ m^{-3} K^{-1}	κ_+ 10^{-7} m^2 s^{-1}	λ_+ W m^{-1} K^{-1}	C_- MJ m^{-3} K^{-1}	κ_- 10^{-7} m^2 s^{-1}	λ_- W m^{-1} K^{-1}	q' W m^{-1}
Loam	1	1.10	4.43	0.49	1.14	4.57	0.52	31.0
	2	1.24	5.09	0.63	1.29	5.32	0.69	30.9
	3	1.36	5.10	0.69	1.47	5.59	0.82	30.9
	4	1.59	5.32	0.85	1.75	5.96	1.04	30.9
Sand	5	1.17	6.49	0.76	1.31	6.60	0.86	31.9
	6	1.40	7.54	1.06	1.49	7.63	1.14	31.5
	7	1.57	7.74	1.21	1.77	7.98	1.41	31.7
	8	1.75	7.74	1.35	2.03	7.85	1.60	32.1

soil columns. First, moist soil samples were prepared according to the designated water contents in the upper and lower soil layers. Secondly, the lower half (40 cm high) of column was packed at the specified bulk density, and the HP sensor was carefully inserted into the column from a pre-drilled a slot at the wall, with the heating probe (H) located at the top of the soil layer, and a sensing probe (S2) inside the soil sample (Fig. 1). Finally, the upper soil layer was carefully packed on top of the lower soil layer. During HP measurements, the heating power (30.9–32.1 W m^{-1}) and the heat pulse length (25 s) were carefully designed to reduce potential water redistribution caused by temperature gradient. After making HP measurements, the upper and lower soil layers were oven dried separately at 105℃ to determine the actual θ and ρ_b values.

2.3. Numerical simulations with the COMSOL Multiphysics module

First, we considered the eight packing scenarios in the COMSOL simulation, and compared the simulation results with those obtained in HP measurements to evaluate the accuracy of the simulated results. Parameters used in the COMSOL simulation were consistent with those in the soil sample experiments (Table 1). The problem domain of COMSOL simulation included two joined rectangular regions (80 × 80 mm) representing the upper and lower soil layers (Fig. 1). The three probes (S1, H, and S2) of a virtual HP sensor were situated in the upper soil layer, at the interface and in the lower soil layer, respectively. The initial condition was set as zero with an adiabatic boundary condition. The heating probe was positioned at the joined interface between the two cuboid regions, and the sensing probes were separately set up in the upper and lower cuboid regions at distances of z_1 and z_2 away from the layer interface. The heating and sensing probes, which consisted of stainless steel and thermally conductive epoxy, with finite radius, finite thermal conductivity and heat capacity, were considered in the simulations (Knight et al., 2012). Simulated results were obtained with the following set of parameters for the sensor configuration and HP measurements: z_1 = 9.87 mm, and z_2 = 9.73 mm. The Peng et al. (2019) sensor configuration was used in the simulations with the radii for the heating probe (r_h) and the sensing probe (r_s) of 2.38 mm and 2 mm, respectively. The heat capacities of the heating probe (C_{p1}) and sensing probe (C_{p2}) were 3.42 MJ m^{-3} K^{-1} and 2.56 MJ m^{-3} K^{-1}, respectively. The measurement time (t) and heating duration (t_0) were set as 250 s and 25 s, respectively. The heat input q' used in the simulations was identical to that used in the laboratory experiments (Table 1). The C and λ values of the soil sample were estimated with the de Vries (1963) C model and the Lu et al. (2014) λ model, respectively, with the information of soil texture and the actual θ and ρ_b values of the upper and lower soil layers. The κ value was calculated as the ratio of λ and C. Table 1 lists the soil thermal property values of upper and lower soil layers used in the simulations.

Second, an additional numerical simulation was conducted to analyze heat transfer during HP measurements, and to evaluate the performances of the hetero-IILS, hetero-PILS, and hetero-CPC models in analyzing the HP measurements in the double-layered soils. The numerical simulations were conducted on two hypothetical soils: a sand (94% sand, 1% silt, 5% clay) and a loam (48% sand, 38% silt, 14% clay). On each soil, 11 scenarios were established to represent various soil thermal property combinations in the double-layered soil columns by varying θ and ρ_b values. Simulated results were obtained with the following set of parameters: r_h = 2.38 mm, r_s = 2 mm, C_{p1} = 3.42 MJ m^{-3} K^{-1}, C_{p2} = 2.56 MJ m^{-3} K^{-1}, t = 250 s, t_0 = 25 s, q' = 31 W m^{-1}, and $z_1 = z_2$ = 10 mm. The input soil C_+, C_-, λ_+ and λ_- were estimated with the de Vries (1963) C model and the Lu et al. (2014) λ model with the selected θ and ρ_b values. The input κ_+ and κ_- values were estimated by dividing λ_+ and λ_- with C_+ and C_-, respectively. Table 2 provides the soil thermal property values of the upper and lower soil layers for the loam soil. The corresponding values of the sand soil are listed in Table S1.

3. Results and discussion

3.1. Comparisons of HP measured and COMSOL simulated temperature-by-time curves

Fig. 2 shows the HP measured and the COMSOL simulated temperature-by-time curves of the double-layered soils. The results of upper and lower soil layers from scenarios 1–4 (Table 1) are shown in Fig. 2a-2d and Fig. 2e-2 h, respectively. For both soil layers, the maximum temperature change (ΔT_{max}) and its arrival time (t_{max}) decreased as the thermal property values (C, κ, λ) increased (Fig. 2). Compared to the upper soil layers, larger λ values in the lower soil layers led to lower t_{max} values (Fig. 2e-h). The ΔT_{max} values of lower soil layers were higher than those of the upper soil layers, which might be caused by the different thermal property values that resulted in heat flux differences at S1 and S2. The COMSOL simulated temperature-by-time curves, which were based on the experimental C and λ results, matched well with the HP sensor measured curves. The COMSOL simulated and HP measured temperature-by-time curves of the sand soil (scenarios 5–8, Table 1), which were presented in Fig. S1, showed consistent results with those on the loam soil.

Some discrepancies between the COMSOL simulated and HP measured temperature-by-time curves occurred, which might be caused by experimental errors during the HP measurements, e.g., probe deflection and water redistribution across the layer interface. In addition, the COMSOL simulation ignores probe-to-soil contact resistance, which may introduce biased estimations.

In general, the COMSOL simulation provided reliable temperature-by-time curves for the different scenarios as described in Table 1. In

Table 2
The 11 scenarios used to represent various thermal property combinations in the double-layered loam soil columns for numerical simulation of heat transfer during HP measurements. Parameters C_+, κ_+, and λ_+ represent the heat capacity (C), thermal diffusivity (κ), and thermal conductivity (λ) of the upper soil layer, respectively, and C_-, κ_- and λ_- represent the corresponding values of the lower soil layer. Parameters A, B, and D represent the ratios of C_+/C_-, κ_+/κ_-, and λ_+/λ_-, respectively.

Scenario	C_+	κ_+	λ_+	C_-	κ_-	λ_-	A	B	D
	MJ m^{-3} K^{-1}	10^{-7} m^2 s^{-1}	W m^{-1} K^{-1}	MJ m^{-3} K^{-1}	10^{-7} m^2 s^{-1}	W m^{-1} K^{-1}			
1	1.02	4.02	0.41	2.08	6.01	1.25	0.49	0.67	0.33
2	1.10	4.43	0.49	1.87	6.58	1.23	0.59	0.67	0.39
3	1.25	4.86	0.61	1.87	6.58	1.23	0.67	0.74	0.50
4	1.25	4.86	0.61	1.46	6.03	0.88	0.86	0.81	0.69
5	1.46	6.03	0.88	1.67	6.47	1.08	0.87	0.93	0.81
6	1.67	6.47	1.08	1.87	6.58	1.23	0.89	0.98	0.88
7	1.10	4.43	0.49	1.25	4.86	0.61	0.88	0.91	0.80
8	1.31	5.34	0.70	1.46	6.03	0.88	0.90	0.89	0.80
9	1.52	5.64	0.86	1.67	6.47	1.08	0.91	0.87	0.80
10	1.73	5.66	0.98	1.87	6.58	1.23	0.93	0.86	0.80
11	1.87	6.58	1.23	1.87	6.58	1.23	1.00	1.00	1.00

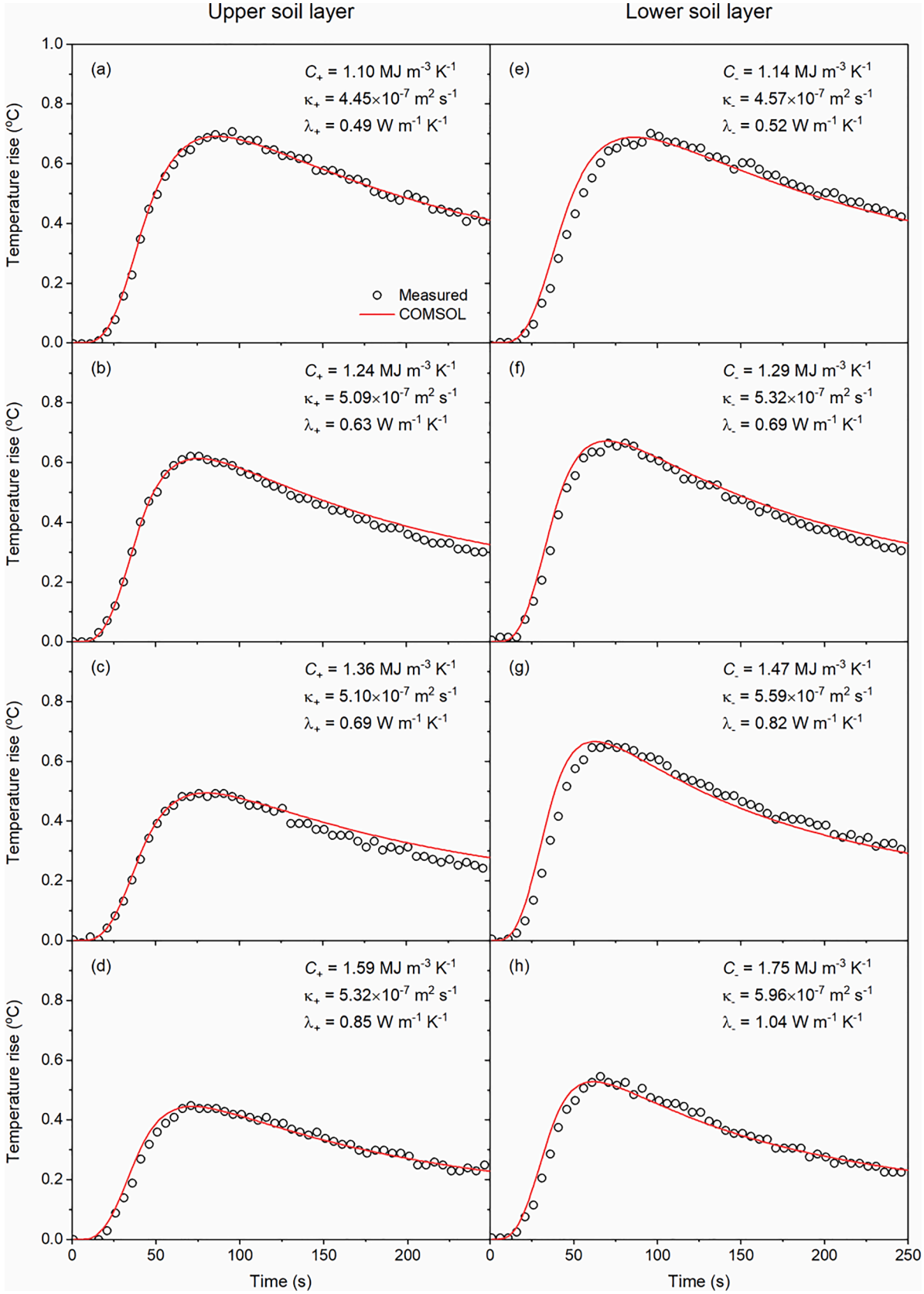

Fig. 2. The heat pulse measured and COMSOL simulated temperature-by-time curves for Scenarios 1–4 presented in Table 1. The (a-d) panels represent the upper soil layer and the (e-h) panels represent the lower soil layer. The black circles are heat pulse measured temperature-by-time curves. The red curves are COMSOL simulated temperature-by-time curves.

the following studies, the COMSOL simulated HP data were used to evaluate the performances of the hetero-IILS, hetero-PILS, and hetero-CPC models for a range of hypothetical conditions.

3.2. Temperature distribution around the sensor for scenario 1

Fig. 3 shows COMSOL simulated temperature distributions around the sensor positioned in a double-layered soil (scenario 1, Table 2) at 100 s after the heat pulse was released. The circles of different colors represented the isotherms in the temperature field around the probes, which were distributed from the center to outside for a temperature interval of 0.15°C. The greatest temperature change appeared near the heating source, the isotherms became semi-circular with different radii in the upper and lower soil layers, and the radii of the isotherm in the upper layer were smaller than those of the lower layer. For example, the temperature ranges at S2 ranged from 0.68°C to 0.83°C, while that ranged from 0.53°C to 0.68°C at S1. Apparently the soil temperature field during HP measurements was distorted due to the different thermal property values of the two soil layers.

The temperature gradient induced heat conduction was reflected in the magnitude of soil heat flux density. Fig. 4 shows the heat flux values at S1 and S2 during the HP measurement. At the t of 100 s, the heat flux density at S2 was two times that at S1, with a maximum heat flux difference of ~ 60 W m^{-1} between the two probe positions (scenario 1, Table 2). With the reduction in thermal property difference between the upper and lower soil layers (i.e., from scenario 1 to scenario 11, Table 2), the magnitude of heat flux difference between S1 and S2 decreased continuously (data not shown). Thus, during HP measurements, the heat transfer process around the HP sensor differed in the upper and lower soil layers, and it was essential to quantify the subsequent consequences on the temperature-by-time curves.

3.3. Comparisons of COMSOL simulated and parameterized models estimated temperature-by-time curves

Fig. 5 shows the COMSOL simulated and numerically calculated (with hetero-IILS, hetero-PILS, and hetero-CPC models) temperature-by-time curves at S1 and S2 at θ values of 0.05, 0.10, 0.15 and 0.20 m^3 m^{-3}

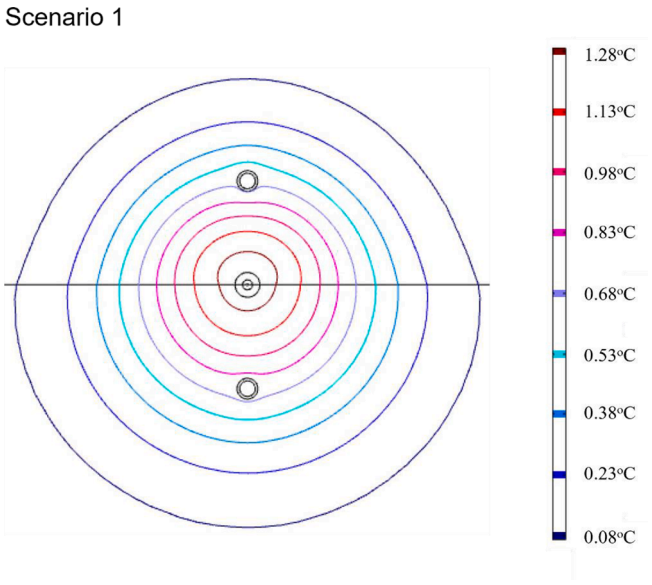

Fig. 3. The COMSOL simulated isotherm around a HP sensor for Scenario 1 presented in Table 2 at the measurement time of 100 s. The heating probe was at the soil layer interface (horizontal black line), and the sensing probes (S1 and S2) were in the upper and lower soil layers at 10 mm away from the interface, respectively.

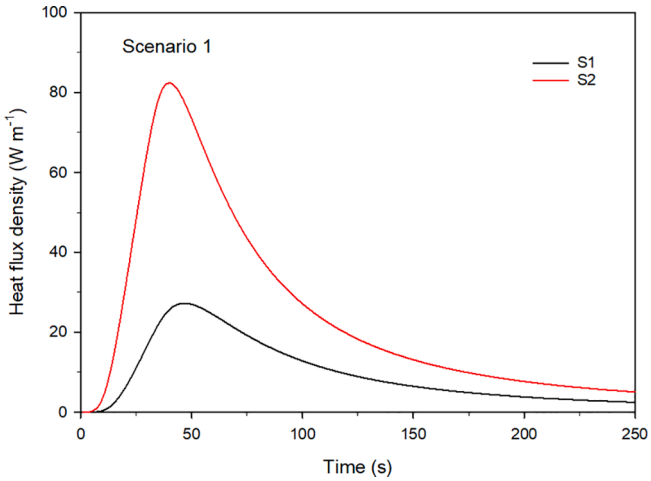

Fig. 4. The COMSOL simulated heat fluxes versus time values at S1 and S2 for Scenario 1 presented in Table 2. S1 and S2 represented the sensing probes in the upper and lower soil layers, respectively.

for the loam soil layers. At each θ value, the dissimilar soil thermal properties were achieved by varying ρ_b values of the upper and lower soil layers, where the lower layer always had greater thermal property values than those of the upper layer (scenarios 7–10, Table 2). The COMSOL simulated and numerically calculated temperature curves varied considerably across the two layers, as manifested in the ΔT_{max} and t_{max} values: Compared to the upper soil layer, larger ΔT_{max} and earlier t_{max} values were observed in the lower soil layer (Fig. 5). For example, at $\theta = 0.05$ m^3 m^{-3}, the simulated ΔT_{max} and t_{max} values were 0.71°C and 82 s for the upper soil layer (Fig. 5a), and the corresponding ΔT_{max} and t_{max} values were 0.75°C and 77 s for the lower soil layer (Fig. 5e). Similar phenomena were also observed in the soil columns packed at the same ρ_b but with different θ values in the upper and lower layers (scenarios 3–6, Table 2), i.e., with higher soil θ values and thus greater thermal property values, the lower soil layer continuously had higher ΔT_{max} and lower t_{max} values than those of the upper soil layer (data not shown).

The hetero-IILS model, which assumes an instantaneous and line heat source (i.e., zero heat pulse length and zero probe diameter and heat capacity), produced HP signals with greater temperature rise and significantly earlier arrival time (Fig. 5), as compared with the COMSOL simulated values. Under scenario 7, for example, the t_{max} arrived 23 s earlier and the ΔT_{max} was 0.04°C higher in the upper soil layer (Fig. 5a). Consequently, the hetero-IILS model would give overestimated κ values and underestimated C values, and the errors were especially apparent in dry soil samples.

By including the finite heat pulse length in model calculation, the hetero-PILS model produce HP signals shifted towards the right size, which coordinated well with the COMSOL simulated results (Fig. 5). However, due to the negligence of the finite probe properties, the temperature rises remained higher than those of COMSOL simulated values. For instance, in Fig. 5a, the hetero-PILS model generated a t_{max} value about 8 s earlier than the COMSOL simulated value, and its ΔT_{max} was 0.04°C higher than that corresponding value from COMSOL simulation (Fig. 5a). Thus, the hetero-PILS model still gave the overestimated κ and underestimated C values, especially in dry soils.

Contrary to the hetero-IILS and hetero-PILS models, the hetero-CPC model performed well in estimating soil thermal properties on the double-layered loam soil samples. For scenarios 7–10 (Table 2), comparing with the COMSOL simulated ΔT_{max} values, the hetero-CPC model gave ΔT_{max} data slightly lower (0.03°C) in the upper soil layer (Fig. 5a-5d), and slightly higher values (0.01°C) in the lower soil layer (Fig. 5e-5 h). These differences were approximate to the measurement accuracy (0.02°C) of the thermocouple temperature sensors and thus

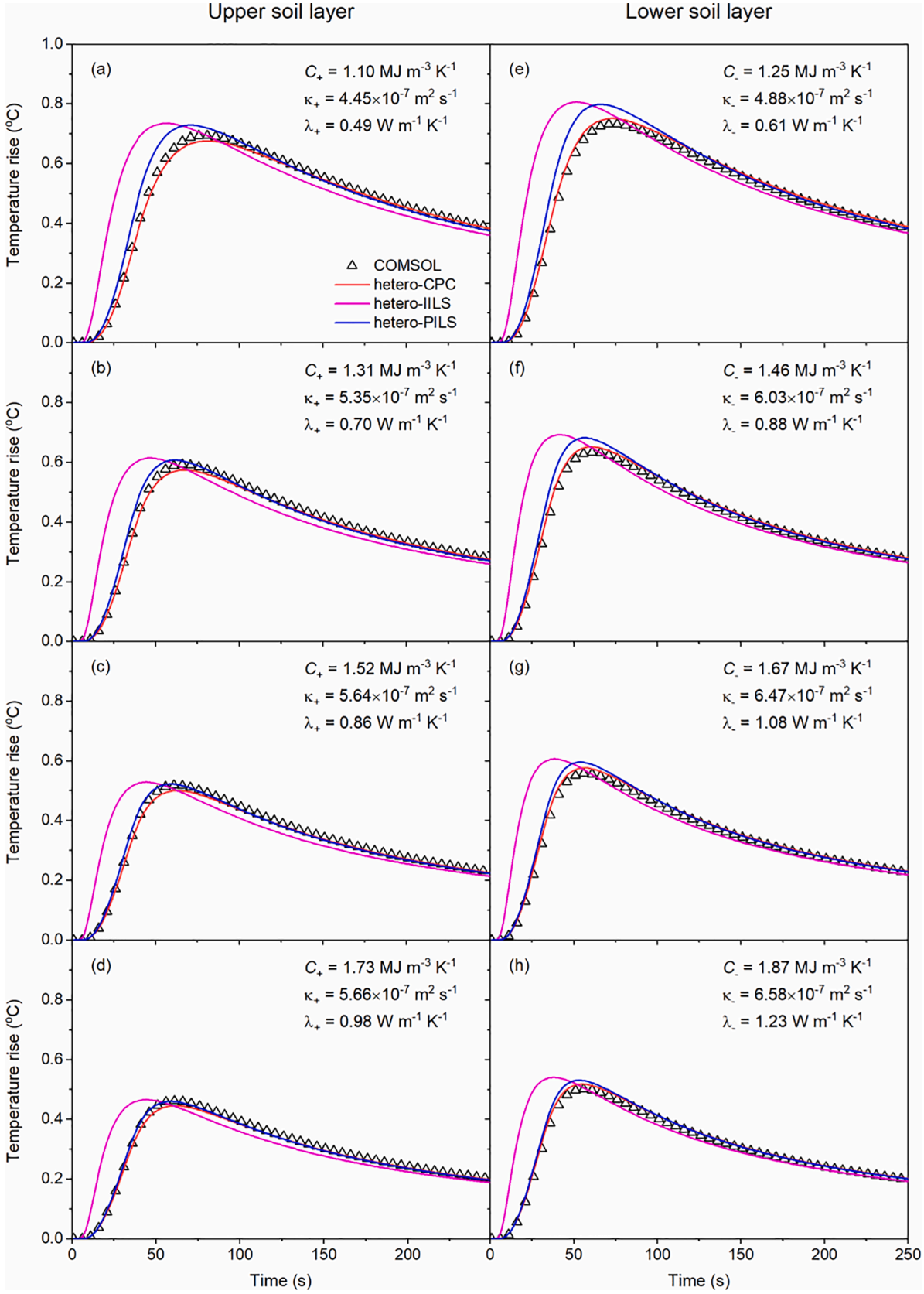

Fig. 5. The temperature-by-time curves of soil layers for Scenarios 7–10 in Table 2. The (a-d) panels represent the upper soil layer and (e-h) panels represent the lower soil layer. The black triangles are COMSOL simulated temperature-by-time curves. The red, blue, and pink lines are the estimated temperature-by-time curves with the hetero-CPC, hetero-PILS, and hetero-IILS models, respectively.

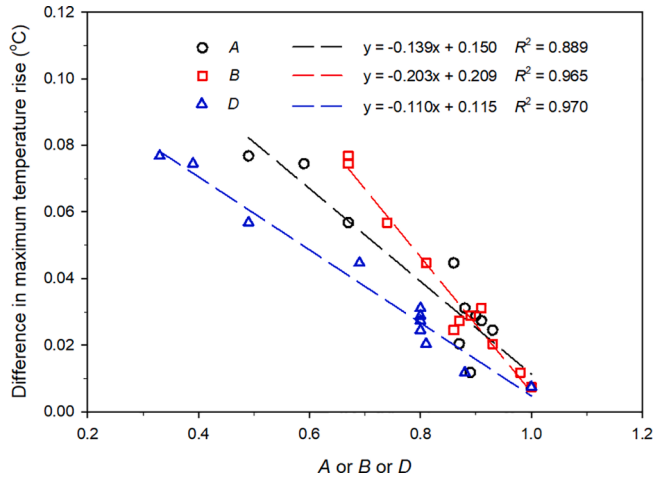

Fig. 6. The difference between hetero-CPC model estimated and COMSOL simulated maximum temperature rise in the upper soil layer as related to the thermal property ratios of upper and lower soil layers. Parameters *A*, *B* and *D* represent the ratios of C_+/C_-, κ_+/κ_-, and λ_+/λ_-.

could be ignored. In addition, the hetero-CPC model calculated and the COMSOL simulated t_{max} differences were < 3 s (Fig. 5), which had minor influences on the κ results.

We also evaluated the performance of the parameterized models on a hypothetical sand soil, and obtained similar results with those on the loam soil (Fig. S2). Under scenarios 7–10 (Table S1), for example, larger ΔT_{max} and earlier t_{max} values were observed in the lower soil layers as compared to the upper soil layers (Fig. S2). Comparing with the COMSOL simulated data, the hetero-IILS and hetero-PILS models gave higher ΔT_{max} values, while the ΔT_{max} errors from the hetero-CPC model were within 0.02°C (Fig. S2). Thus, the hetero-CPC model was able to provide relatively accurate temperature-by-time curves and thermal property results in double-layered soils, irrespective of soil textures, water content, and bulk density.

Finally, we compared the performance of the hetero-CPC model in the upper and lower soil layer with a wide range of thermal property contrast, as illustrated in the 11 scenarios (Table 2). Parameters *A*, *B*, and *D*, which represented the ratios of C_+/C_-, κ_+/κ_-, and λ_+/λ_-, respectively, ranged from 0.33 to 0.67 in scenario 1 (i.e., the two layers had the largest thermal contrast), and were equal to 1 in scenario 11 (i.e., the two layers had identical thermal properties). In the lower soil layer that had equal or greater thermal properties than the upper layer, the differences between hetero-CPC estimated and COMSOL simulated ΔT_{max} values were within 0.03°C, indicating that soil heterogeneity of the double-layered system had negligible effects on the heat capacity results. In the upper soil layer, however, the temperature-by-time curves were notably altered by soil heterogeneity: The hetero-CPC estimated ΔT_{max} values were lower than those obtained from COMSOL simulation; the larger in thermal property contrast between the two layers, the more difference between the ΔT_{max} data. Regression analysis revealed linear relationships between the ΔT_{max} differences and the thermal property ratios (i.e., *A*, *B*, and *D*), with coefficients of determination (R^2) > 0.89 (Fig. 6). The differences in hetero-CPC estimated and COMSOL simulated ΔT_{max} increased with decreasing *A*, *B*, and *D* values (Fig. 6). The maximum error of the hetero-CPC model occurred in scenario 1 (Table 2) with thermal property values at dry and saturated conditions for the upper and lower soil layers, respectively. Thus, for the two-layer soil system considered in this study, more temperature field distortion (and therefore larger thermal property errors) occurred in the low-thermal property side, and relatively accurate results were expected in the high-thermal property part. Clearly, the linear relationship depicted in Fig. 6 implied its possible use in quantifying the errors from the hetero-CPC modeled temperature-by-time curves using the soil thermal property contrast in layered soil systems. Further evaluations should be conducted to test the hetero-CPC model under a wide range of heterogeneous soil conditions, and to evaluate the feasibility of the hetero-CPC model for estimating soil thermal property values.

4. Conclusions

In this study, we analyzed heat transfer patterns around a HP sensor building upon the Philip and Kluitenberg (1999) theory to parameterize the CPC theory by positioning the sensor in a double-layered soil. During HP measurements, heat flux distributed differently in the upper and lower soil layers with the heating probe at the soil layer interface, and the heat flux difference became larger as thermal property difference increased. Biased temperature-by-time results were obtained with the traditional hetero-IILS and hetero-PILS models. The proposed hetero-CPC model, which considered heat pulse length and the finite probe properties, accurately captured the temperature-by-time curves at the sensing probes in the upper and lower soil layers. The performance of the hetero-CPC model was related to the thermal property differences between the two soil layers, showing relatively larger errors in estimated temperature signals as the thermal property difference between the upper and lower increased.

Declaration of Competing Interest

The authors declare that they have no known competing financial interests or personal relationships that could have appeared to influence the work reported in this paper.

Acknowledgements

This research was supported by the National Natural Science Foundation of China (41977011 and 41671223), the U.S. National Science Foundation (2037504) and USDA-NIFA Multi-State Project 4188.

Appendix

Philip and Kluitenberg (1999) presented an instantaneous infinite line source theory for the HP sensor located at the interface of two soil layers as depicted in Fig. 1. The S1 and S2 probes locate in upper and lower soil layers, and solutions for the upper and lower soil layers were (hereafter referred to as the hetero-IILS model) as follows,

$$\Delta T1(z_1,t) = \frac{q'}{2\pi(\lambda_+ + \lambda_-)t}\left[\exp\left(\frac{-z_1^2}{4\kappa_+ t}\right)\right] \quad [A1]$$

$$\Delta T2(z_2,t) = \frac{q'}{2\pi(\lambda_+ + \lambda_-)t}\left[\exp\left(\frac{-z_2^2}{4\kappa_- t}\right)\right] \quad [A2]$$

where $\Delta T1(z_1, t)$ and $\Delta T2(z_2, t)$ are the temperature rise at time *t* of the sensing probes located at z_1 and z_2 in upper and lower soil layers, respectively.

q' is the heat input per unit length per unit time (W m^{-1}). λ_+ and λ_- are the soil thermal conductivity values of the upper and lower soil layers (W m^{-1} K^{-1}), respectively. κ_+ and κ_- are the soil thermal diffusivity values of the upper and lower soil layers (m^2 s^{-1}), respectively.

In practice, a short duration heat pulse, not instantaneous heating, is used for HP measurements (Bristow et al., 1994). In the double-layered soil study with the heating probe positioned at the layer interface, we present the following hetero-PILS model with the same parameterization as that in Eqs. [A1] and [A2] to consider a heat pulse duration (t_0),

$$\Delta T1(z_1,t)=\frac{q'}{2\pi(\lambda_+ +\lambda_-)}\left[\mathrm{Ei}\left(\frac{-z_1^2}{4\kappa_+(t-t_0)}\right)-\mathrm{Ei}\left(\frac{-z_1^2}{4\kappa_+ t}\right)\right];t>t_0 \quad [A3]$$

$$\Delta T2(z_2,t)=\frac{q'}{2\pi(\lambda_+ +\lambda_-)}\left[\mathrm{Ei}\left(\frac{-z_2^2}{4\kappa_- (t-t_0)}\right)-\mathrm{Ei}\left(\frac{-z_2^2}{4\kappa_- t}\right)\right];t>t_0 \quad [A4]$$

where -Ei(-x) is the exponential integral.

The hetero-IILS and hetero-PILS models both ignore the effects of finite probe properties during the HP data analysis. Knight et al. (2012) present CPC theory with a semi-analytical solution accounting for the finite probe radius (r) and finite probe heat capacity (C_p). For the case of continuous heating, a Laplace transform expression of the sensing probe temperature at a known distance from the centerline of the infinite cylindrical heat source is,

$$\begin{cases}\widehat{V}(p)=\widehat{v}_f(p,r_h,\beta_1)\widehat{v}_f(p,r_s,\beta_2)\dfrac{q'K_0(\mu z)}{2\pi\lambda p}\\ \widehat{v}_f(p,r_h,\beta_1)=\dfrac{1}{\mu r_h[K_1(\mu r_h)+(\mu r_h\beta_1/2)K_0(\mu r_h)]}\\ \widehat{v}_f(p,r_s,\beta_2)=\dfrac{1}{\mu r_s[K_1(\mu r_s)+(\mu r_s\beta_2/2)K_0(\mu r_s)]}\end{cases} \quad [A5]$$

where z is the distance between heating and sensing probes. r_h is the radius of the heating probe, and r_s is the radius of the sensing probe, $\beta_1=C_{p1}/C$ and $\beta_2=C_{p2}/C$, where C_{p1} and C_{p2} are the heat capacity of the heating and sensing probes, respectively; $K_u(i)$ denotes the modified Bessel function of the second kind of order u and argument i;$\mu=\sqrt{p/\kappa}$, where p is the Laplace transform parameter; $\widehat{V}(p)$ is the Laplace transform of $V(t)$, which is the temperature of the sensing probe; The $\widehat{v}_f=(p,r_h,\beta_1)$ and $\widehat{v}_f=(p,r_s,\beta_2)$ are the corresponding transfer functions. The Laplace domain solution, Eq. [A5], is numerically inverted for two cases: $V(t)$ and $V(t-t_0)$ using the algorithm of Stehfest (1970a, 1970b). For the case of pulsed heating, the corresponding expression is,

$$V^{\mathrm{P}}(t)=\begin{cases}V(t);0<t\leqslant t_0\\ V(t)-V(t-t_0);t>t_0\end{cases} \quad [A6]$$

For the double-layered soil condition in Fig. 1, we propose a hetero-CPC model by introducing parameters of λ_+, λ_-, z_1, μ_1, β_{11}, β_{12}, z_2, μ_2, β_{21} and β_{22} into the CPC solution (Knight et al., 2012; Eq. [A5]). Referring to the hetero-PILS model, the λ in Eq. [A5] is replaced by the average of λ_+ and λ_- for the double-layered soil. For the upper soil layer, the parameters of z, μ, β_1 and β_2 in Eq. [A5] are replaced by z_1, μ_1, β_{11} and β_{12} in which$\mu_1=\sqrt{p/\kappa_+}$, $\beta_{11}=C_{p1}/C_+$, $\beta_{12}=C_{p2}/C_+$. For the lower soil layer, the parameters of z, μ, β_1 and β_2 in Eq. [A5] are replaced by z_2, μ_2, β_{21} and β_{22}, in which$\mu_2=\sqrt{p/\kappa_-}$, $\beta_{21}=C_{p1}/C_-$ and $\beta_{22}=C_{p2}/C_-$. The semi-analytical solution becomes,

$$\widehat{V}1(p)=\widehat{v}_f(p,r_h,\beta_{11})\widehat{v}_f(p,r_s,\beta_{12})\frac{q'K_0(\mu_1 z_1)}{\pi(\lambda_+ +\lambda_-)p} \quad [A7]$$

$$\widehat{V}2(p)=\widehat{v}_f(p,r_h,\beta_{21})\widehat{v}_f(p,r_s,\beta_{22})\frac{q'K_0(\mu_2 z_2)}{\pi(\lambda_+ +\lambda_-)p} \quad [A8]$$

where $\widehat{V}1(p)$ and $\widehat{V}2(p)$ are the Laplace transforms of $V1(t)$ and $V2(t)$, which are the temperature-by-time of the sensing probes in the upper and lower soil layers, respectively. Equations [A6-A8] are the solutions for a double-layered soil condition where the heating probe is positioned at the layer interface. The hetero-PILS (Eqs. [A3-A4]) and hetero-CPC (Eqs. [A7-A8]) are newly proposed solutions in this study.

Appendix A. Supplementary data

Supplementary data to this article can be found online at https://doi.org/10.1016/j.geoderma.2022.115987.

References

Bristow, K.L., Kluitenberg, G.J., Horton, R., 1994. Measurement of soil thermal properties with a dual-probe heat-pulse technique. Soil Sci. Soc. Am. J. 58 (5), 1288–1294.

Campbell, G.S., Calissendorff, C., Williams, J.H., 1991. Probe for measuring soil specific heat using a heat-pulse method. Soil Sci. Soc. Am. J. 55 (1), 291–293.

de Vries, D.A., 1963. Thermal properties of soils. In: Van Wijk, W.R. (Ed.), Physics of plant environment. North-Holland Publ. Co., Amsterdam.

Gamage, D.N.V., Biswas, A., Strachan, I.B., 2019. Spatial variability of soil thermal properties and their relationships with physical properties at field scale. Soil Till. Res. 193, 50–58.

Gee, G.W., Or, D., 2002. Particle-size analysis. In: J.H. Dane and G.C. Topp, editors, Methods of soil analysis. Part. 4. SSSA, Madison, WI. p. 255-293.

He, H., Dyck, M.F., Horton, R., Ren, T., Bristow, K.L., Lv, J., Si, B., 2018. Development and application of the heat pulse method for soil physical measurements. Rev. Geophys. 56 (4), 567–620.

Kamai, T., Kluitenberg, G.J., Hopmans, J.W., 2015. A dual-probe heat-pulse sensor with rigid probes for improved soil water content measurement. Soil Sci. Soc. Am. J. 79 (4), 1059–1072.

Kluitenberg, G.J., Ham, J.M., Bristow, K.L., 1993. Error analysis of the heat pulse method for measuring soil volumetric heat capacity. Soil Sci. Soc. Am. J. 57 (6), 1444–1451.
Kluitenberg, G.J., Philip, J.R., 1999. Dual thermal probes near plane interfaces. Soil Sci. Soc. Am. J. 63 (6), 1585–1591.
Kluitenberg, G.J., Bristow, K.L., Das, B.S., 1995. Error analysis of the heat pulse method for measuring soil heat capacity, diffusivity, and conductivity. Soil Sci. Soc. Am. J. 59, 719–726.
Kluitenberg, G.J., Knight, J.H., Kamai, T., 2021. Integral form of the cylindrical perfect conductors solution for the dual-probe heat-pulse method. Soil Sci. Soc. Am. J. 85 (6), 1963–1969.
Knight, J.H., Kluitenberg, G.J., Kamai, T., Hopmans, J.W., 2012. Semianalytical solution for dual-probe heat-pulse applications that accounts for probe radius and heat capacity. Vadose Zone J. 11 (2).
Liu, G., Zhao, L., Wen, M., Chang, X., Hu, K., 2013. An adiabatic boundary condition solution for improved accuracy of heat-pulse measurement analysis near the soil–atmosphere interface. Soil Sci. Soc. Am. J. 77 (2), 422–426.
Liu, G., Lu, Y., Wen, M., Ren, T., Horton, R., 2020. Advances in the heat-pulse technique: Improvements in measuring soil thermal properties. Soil Sci. Soc. Am. J. 84 (5), 1361–1370.
Lu, Y., Lu, S., Horton, R., Ren, T., 2014. An empirical model for estimating soil thermal conductivity from texture, water content, and bulk density. Soil Sci. Soc. Am. J. 78 (6), 1859–1868.
Peng, W., Lu, Y., Xie, X., Ren, T., Horton, R., 2019. An improved thermo-TDR technique for monitoring soil thermal properties, water content, bulk density, and porosity. Vadose Zone J. 18 (1), 1–9.
Peng, W., Lu, Y.L., Ren, T.S., Horton, R., 2021. Application of infinite line source and cylindrical-perfect-conductor theories to heat pulse measurements with large sensors. Soil Sci. Soc. Am. J. 85, 1050–1059.
Peters-Lidard, C.D., Blackburn, E., Liang, X., Wood, E.F., 1998. The effect of soil thermal conductivity parameterization on surface energy fluxes and temperatures. J. Atmos. Sci. 55 (7), 1209–1224.
Philip, J.R., Kluitenberg, G.J., 1999. Errors of dual probes due to soil heterogeneity across a plane interface. Soil Sci. Soc. Am. J. 63, 1579–1585.
Sang, Y., Liu, G., Horton, R., 2020. Wind effects on soil thermal properties measured by the dual-probe heat pulse method. Soil Sci. Soc. Am. J. 84 (2), 414–424.
Stehfest, H., 1970a. Algorithm 368: Numerical inversion of Laplace transforms. Commun. ACM 13, 47–49.
Stehfest, H., 1970b. Remark on Algorithm 368: Numerical inversion of Laplace transforms. Commun. ACM 13 (10), 624.
Xiao, X., Zhang, X., Ren, T., Horton, R., Heitman, J.L., 2015. Thermal property measurement errors with heat-pulse sensors positioned near a soil-air interface. Soil Sci. Soc. Am. J. 79 (3), 766–771.
Xie, X.T., Lu, Y.L., Ren, T.S., Horton, R., 2019. Soil temperature estimation with the harmonic method is affected by thermal diffusivity parameterization. Geoderma 353, 97–103.
Zhang, X., Heitman, J., Horton, R., Ren, T., 2014. Measuring near-surface soil thermal properties with the heat-pulse method: Correction of ambient temperature and soil-air interface effects. Soil Sci. Soc. Am. J. 78 (5), 1575–1583.